



Multiple Assembly States of Lumazine Synthase: A Model Relating Catalytic Function and Molecular Assembly

**Xiaofeng Zhang^{1†}, Petr V. Konarev^{2†}, Maxim V. Petoukhov²
Dmitri I. Svergun^{2*}, Li Xing³, R. Holland Cheng^{3,4}, Ilka Haase⁵
Markus Fischer⁵, Adelbert Bacher⁵, Rudolf Ladenstein¹
and Winfried Meining^{1*}**

¹Karolinska Institutet
Department of Biosciences
Center for Structural
Biochemistry, S-14157
Huddinge, Sweden

²European Molecular Biology
Laboratory, Hamburg
Outstation, Notkestrasse 85
22603 Hamburg, Germany
and Institute of Crystallography
Russian Academy of Sciences
Leninsky pr. 59
117333 Moscow, Russia

³University of California
Molecular and Cellular Biology
Davis, CA 95616, USA

⁴Karolinska Institutet
Department of Biosciences
Center for Biotechnology
S-14157 Huddinge, Sweden

⁵Lehrstuhl für Organische
Chemie und Biochemie
Technische Universität
München, Lichtenbergstr. 4
D-85747 Garching, Federal
Republic of Germany

*Corresponding authors

Lumazine synthases have been observed in the form of pentamers, dimers of pentamers, icosahedral capsids consisting of 60 subunits and larger capsids with unknown molecular structure. Here we describe the analysis of the assembly of native and mutant forms of lumazine synthases from *Bacillus subtilis* and *Aquifex aeolicus* at various pH values and in the presence of different buffers using small angle X-ray scattering and electron microscopy. Both wild-type lumazine synthases are able to form capsids with a diameter of roughly 160 Å and larger capsids with diameters of around 300 Å. The relative abundance of smaller and larger capsids is strongly dependent on buffer and pH. Both forms can co-exist and are in some cases accompanied by other incomplete or deformed capsids. Several mutants of the *B. subtilis* lumazine synthase, in which residues in or close to the active site were replaced, as well as an insertion mutant of *A. aeolicus* lumazine synthase form partially or exclusively larger capsids with a diameter of about 300 Å. The mutations also reduce or inhibit enzymatic activity, suggesting that the catalytic function of the enzyme is tightly correlated with its quaternary structure. The data show that multiple assembly forms are a general feature of lumazine synthases.

© 2006 Elsevier Ltd. All rights reserved.

Keywords: lumazine synthase; electron microscopy; small angle X-ray scattering; multiple assembly states

Introduction

† Contributed equally to this work.

Abbreviations used: LS, lumazine synthase; LSBS, LS from *B. subtilis*; LAAQ, LS from *A. aeolicus*; SAXS, small-angle XC-ray scattering; EM, electron microscopy; LSSC, LS from *S. cerevisiae*.

E-mail addresses of the corresponding authors:
svergun@embl-hamburg.de; winfried.meining@csb.ki.se

The ability of proteins to assume different quaternary structures is essential for many biological processes such as signal transduction, cell-cycle regulation and enzyme catalysis. Among factors that trigger the change of quaternary structure are temperature shifts, change of ionic strength, pH and binding of ligands. In some

cases protein engineering such as cleavage, mutation and insertion leads to a change of folding or assembly patterns *in vitro*.^{1,2} Macromolecular assemblies following icosahedral symmetry share the advantage of being constituted by a comparatively low number of unique building blocks while theoretically being able to form a large number of stable assembly types. The foundations used to explain structural stability of icosahedral macromolecular assemblies were laid down in the theory of quasi-equivalence introduced by Caspar and Klug.³ Many viral assemblies are characterized by the optimization of inter-subunit contacts following the geometric principles of icosahedral quasi-equivalence. Caspar and Klug pointed out that a quasi-equivalent icosahedral capsid can be constructed by introducing pentamers into a surface lattice of hexamers, thus generating a bent shell with icosahedral symmetry.³ The triangulation number (T) indicates the number of subunits in the icosahedral asymmetric unit. The number of subunits in the whole icosahedral particle is thus equal to $60T$ (for a review see Johnson & Speir).⁴

Lumazine synthase (LS) (for a review see Bacher and Ladenstein, or Ladenstein *et al.*)^{5,6} catalyzes the formation of 6,7-dimethyl-8-ribityllumazine in the penultimate step of riboflavin biosynthesis (Figure 1).⁷ In *Saccharomyces cerevisiae*, *Schizosaccharomyces pombe*, *Magnaporthe grisea* and *Mycobacterium tuberculosis* the enzyme forms pentamers, whereas in *Bacillus subtilis*, *Escherichia coli*, *Spinacia oleracea* and *Aquifex aeolicus*, the enzyme forms icosahedral capsids with a diameter of about 160 Å.^{8–15} In the crystallographic unit cell of the structures of *Brucella abortus* LS and *Mycobacterium tuberculosis* two pentamers are tightly attached to each other.^{15–17} Zylberman *et al.* concluded from light scattering studies that the *B. abortus* LS assembles to dimers even in solution.¹⁷ Icosahedral LSs are built up by 60 subunits arranged in 12 pentamers, which constitute a $T=1$ icosahedral capsid with a total molecular mass of about 960 kDa. In icosahedral LSs the first seven N-terminal residues form an inter-subunit β-sheet with the neighboring monomer. In *B. subtilis* lumazine synthase (LSBS), the capsid encloses a trimer of riboflavin synthase (RS), thus forming a

bifunctional enzyme complex, which was formerly named heavy riboflavin synthase.¹⁸ The comparison of known structures of LSs shows that the subunit folds of the pentameric and icosahedral LS are very similar.¹² One monomer comprises a four-stranded β-sheet flanked by two α-helices on one side and three α-helices on the other side. Besides pentamers and the $T=1$ icosahedral capsids, earlier experiments involving a pH-induced dissociation have revealed another assembly form of LS, whose molecular structure, however, has so far remained unclear.¹⁹ Heavy riboflavin synthase was observed to reassemble to large hollow capsids with a diameter of about 330 Å in Tris hydrochloride buffer at pH values greater than 7.5. It was further observed that the substrate analogue, 5-nitroso-6-ribitylamino-2,4(1H,3H)-pyrimidinedione, triggers the reassociation of large particles to empty $T=1$ capsids.

The active sites of LS are located at the interfaces of two adjacent subunits within a pentamer. In icosahedral lumazine synthases, the active site is situated at the inner surface of the capsid close to the icosahedral 2-fold axis, which relates two adjacent pentamer units. The highly conserved residue Arg127 is essential for binding of one of the substrates, L-3,4-hydroxy-2-butanone-4-phosphate ((b), Figures 1 and 2, Arg127 is numbered according to the LSBS sequence; unless stated otherwise, the residue numbers in the following are derived from the sequence of LSBS). This binding site is formed by Arg127 and main chain atoms of three other residues (Gly84, Ala85 and Thr86) of the adjacent subunit. Two other residues, namely Phe57 and Phe113, which belong to different subunits, are known to be crucial for binding of the second substrate 5-amino-6-ribitylamino-2,4(1H,3H)-pyrimidinedione ((a), Figures 1 and 2).²⁰ Both residues form hydrogen bonds *via* main chain atoms to hydroxyl groups of the ribityl side-chain of substrate (a) (Figure 2).^{8,12,13,21} In LSBS and *A. aeolicus* lumazine synthase the aromatic rings of Phe57 and Phe113 are in offset stacking conformation at a distance of about 3.6 Å between the two rings. The aromatic interaction of these two stacking ring systems has thus a stabilizing effect on the subunit interface.

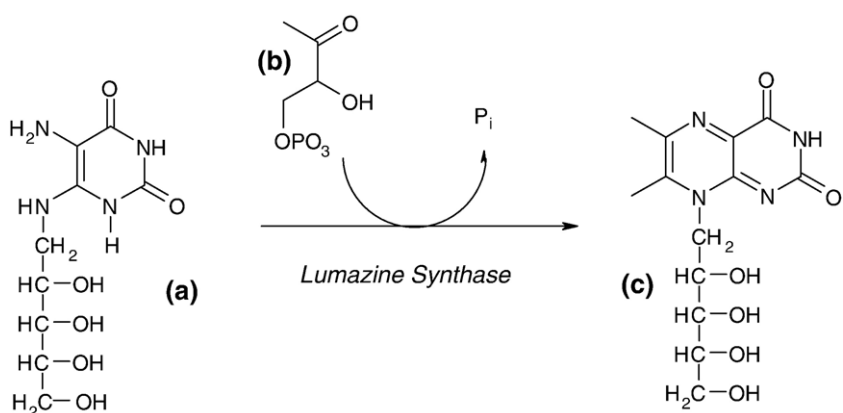


Figure 1. Biosynthesis of 6,7-dimethyl-8-ribityllumazine. (a) 5-Amino-6-ribitylamino-2,4(1H,3H)-pyrimidinedione; (b) 3,4-dihydroxy-2-butanone 4-phosphate; (c) 6,7-dimethyl-8-ribityllumazine.

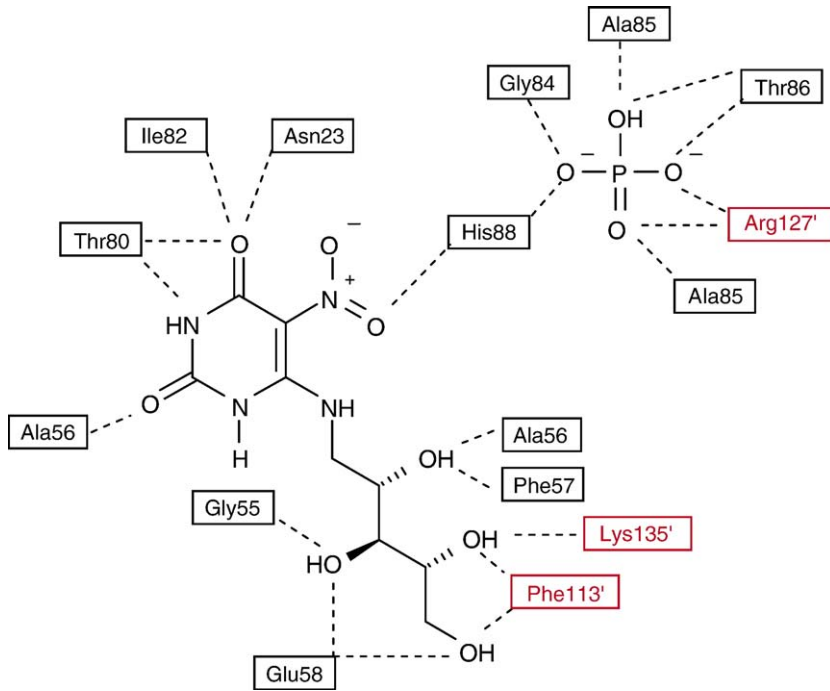


Figure 2. A schematic drawing of the interactions between LSBS and the substrate analogue 6-ribitylamino-5-nitro-2,4(1H,3H)-pyrimidinedione and the phosphate ion. Enzyme residues from two neighboring subunits are colored black and red.²¹

An electrostatic energy analysis indicated that the capsid is stabilized upon binding of the substrate analogue, 5-nitroso-6-ribitylamino-2,4(1H,3H)-pyrimidinedione.²² Thermal unfolding experiments have revealed extraordinary stability of the icosahedral species. The apparent melting temperature (T_m) of the icosahedral LS from the hyperthermophilic bacterium *A. aeolicus* (LSAQ) is 120 °C, which is one of the highest melting temperatures for proteins reported to date. Surprisingly, LS from the mesophilic bacterium *B. subtilis* also displayed an unusual heat tolerance as the T_m reaches 93 °C, whereas the pentameric yeast LS had an apparent melting temperature of 74 °C.¹³ The unusual heat tolerance of icosahedral LS indicates a considerable contribution of capsid formation to their thermal stability.

The question what structural features would lead to pentameric LS or icosahedral LS was investigated and discussed in a number of studies. Braden *et al.* proposed that LSs with a phenylalanine (Phe22) at the active site and a five residue kink, i.e. GT(G)KAG in the C-terminal helix, have potential for capsid formation.¹⁶ Persson *et al.* suggested that an extra residue Pro8 (*M. grisea* LS numbering) at the N-terminal end would break the β -strand, which in icosahedral LSs aligns with the β -sheet of the adjacent subunit, and lead to the formation of pentamers.¹¹ In icosahedral LS the loop linking helix α_4 and helix α_5 is positioned at the interface between two pentameric units of the capsid. A sequence alignment showed that an insertion of one to four residues after Gly133, which is positioned between helices α_4 and α_5 in the hitherto determined LS structures, is unique for all pentameric LS.¹⁰ Computer-modelling studies revealed that a four residues insertion (IDEA) in the *S. cerevisiae* LS (LSSC) in the loop linking helix α_4 and helix α_5 would lead to severe clashes at the subunit interface

in a modeled icosahedral arrangement of pentamers, indicating that the insertion could be responsible for the inability of LSSC to assemble to an icosahedral capsid.¹² Fornasari *et al.* systematically analyzed sequence similarities of lumazine synthases from different species and correlated them with the quaternary structures.²³ Eight sequence sites, which appear to be determinants for icosahedral assembly, were identified.

As the active site of icosahedral LS is located close to the inner surface of the capsid, substrates and products need to be transported to and from the active site through a rather densely packed capsid wall. The largest openings in icosahedral lumazine synthases are channels with a diameter of 5–12 Å located along the icosahedral 5-fold axes. The attempt to block the channels of heavy riboflavin synthase (the LS and RS complex) from *B. subtilis* with a C₅-symmetric tungsten compound resulted in unperturbed enzymatic activity, implying that the transport of substrates and products might follow another pathway.²⁴

Here, the particle distribution of icosahedral capsids of LSBS and LSAQ is analyzed by synchrotron small angle X-ray scattering (SAXS) and electron microscopic methods. The SAXS method reveals the overall structure of macromolecules in solution and also permits us to quantitatively characterize mixtures containing particles of different sizes.²⁵ Application of SAXS allowed us to observe multiple assembly states of LS and selected LS mutants and to systematically analyze pH-induced capsid dissociation and association of the enzyme in different buffers. The data from the electron microscopic analysis complement and support the data obtained by SAXS. A hypothesis of the interplay of enzymatic catalysis and different assembly states of the capsid is proposed.

Results and Discussion

Single-site mutations of lumazine synthase from *B. subtilis*

A number of single-site mutations of LSBS have been shown both to exhibit reduced enzyme activity and to form large capsids (Figure 3 shows the affected residues in their secondary structure environment).²⁰ The residues Phe57 and Phe113 from two adjacent subunits of the same pentamer are in offset stacking interaction with each other. A proper interaction between these residues might be important for the assembly of pentamers. Furthermore, both residues establish main chain hydrogen bonds with hydroxyl groups of substrate (a), making a proper alignment of their main chain atoms crucial for substrate binding. The replacement of either Phe57 or Phe113 with a serine causes

reductions of the reaction rate to 36% and 5%, respectively.²⁰ These two mutants assemble both $T=1$ icosahedral capsids and large capsids as shown by native gel electrophoresis and subsequent Western blotting (I. H. et al., unpublished results). The replacement of Phe57 or Phe113 with a much smaller serine introduces an extra internal cavity in the protein and thus, energetically, has a negative effect on the stabilization of the pentamer.

Arg21 is situated at the subunit interface between two different pentamers and is known to be involved in a highly conserved inter-pentamer ion-pair network found in all icosahedral LSs. Earlier structural studies suggested that this particular ion-pair network is important for the assembly of $T=1$ icosahedral capsids.¹³ Zhang et al. proposed that Arg21 is important for assembly of the $T=1$ capsid.¹³ The replacement of Arg21 by a hydrophobic alanine would disrupt the charge-charge interaction at the subunit interface between two

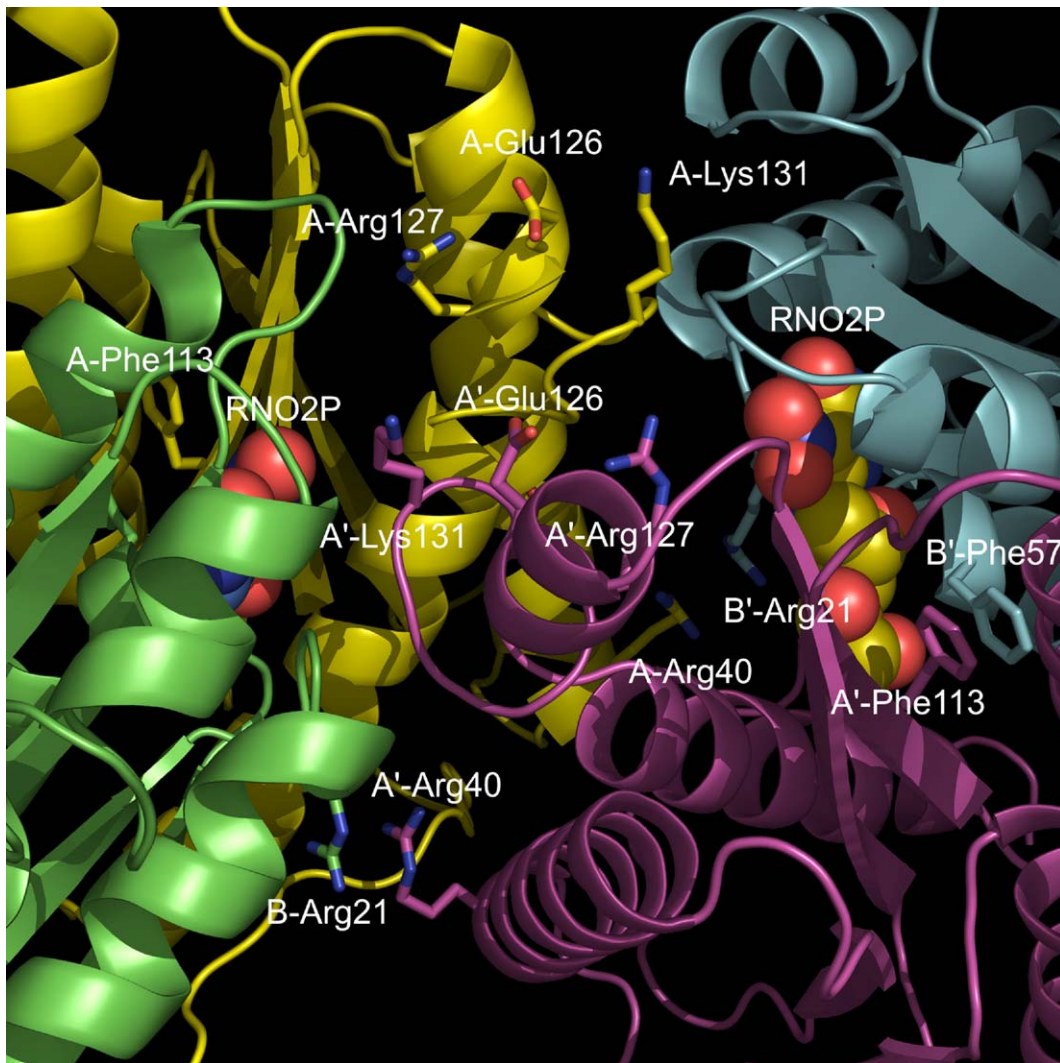


Figure 3. Ribbon representation of the pentamer–pentamer interface of lumazine synthase from *B. subtilis* (PDB ID: 1rvv) with some residues shown in sticks representation.³⁸ The yellow and green subunits belong to one pentamer and the blue and magenta subunits to the other. The pentamer–pentamer interface encloses a 2-fold axis, which relates subunit A with A' and subunit B with B'. The residues Arg21, Phe57, Phe113, and Arg127 were mutated for the purpose of this study. The ligand RNO2P (5-nitro-6-ribityl-amino-2,4(1h,3h)-pyrimidinedione) is shown as CPK model.

adjacent pentamers and therefore may affect the capsid assembly. The mutant Arg21Ala assembles both $T=1$ and large capsids and has about 43% residual catalytic activity with respect to the wild-type LSBS.

Arg127 in the active site is known to play a crucial role for substrate binding and the catalytic activity of the enzyme.²⁰ This residue is responsible for binding of the phosphorylated substrate (b) (Figure 2) before the reaction commences. In all known structures of LS, either a phosphate anion or an inhibitor carrying a phosphonate group is bound to this arginine residue. Furthermore, Arg127, Glu126 and Lys131 form an ionic network, which extends to a surface region opposite to the adjacent pentamer unit.²¹ The replacement of Arg127 by a polar, hydrophobic or acidic residue results in more than 95% reduction of catalytic activity with respect to the wild-type enzyme.²⁰ The Arg127Thr mutant is not catalytically active, whereas the activity of the Arg127His mutant is reduced to 62%. Both Arg127His and Arg127Thr form capsids of at least two different sizes, one resembling the known $T=1$ capsid and the others with a diameter of at least 280 Å. Whereas the native enzyme forms exclusively small capsids (Figure 4(a)), Arg127His forms mostly small capsids and only to a minor extent large capsids (Figure 4(b)), and the mutant Arg127Thr forms mostly large capsids (Figure 4(c)). Histidine may still bind to phosphate via ionic interactions and thus help to maintain residual catalytic activity, whereas threonine cannot take part in an ionic interaction. Due to its basic character histidine is also able to mimick electrostatic interactions of arginine, which could help to maintain subunit interactions that are responsible for quaternary assembly.

As substrate (b) also forms hydrogen bonds with residues Gly84, Ala85 and Thr86 from the adjacent subunit, the removal of Arg127 not only affects the substrate binding site for the substrate but also the hydrogen bond contacts between the two subunits that are formed via the bound substrate (b). These observations suggest that substrate or phosphate

binding stabilizes the subunit contacts within pentamers. Thus, if the binding site is disturbed or destroyed, the pentameric blocks of the $T=1$ capsid will be destabilized.

Analysis of wild-type and mutants of lumazine synthases by cryoelectron microscopy

The inspection of various samples of native and modified LSs by SAXS methods showed that LS particles appear to have diameters in three different ranges, 160–200 Å (type I), 270–300 Å (type II) and 300–330 Å (type III). Whereas the SAXS studies indicate the presence of distinct type II and type III particles, none of the samples investigated by electron microscopy (EM) methods allows the unambiguous distinction of type II from type III particles. In the context of presenting data from EM studies we therefore merge counts for type II and type III particles.

In phosphate buffer (pH 8.0), LSBS forms exclusively type I particles (Figure 5(a), Table 1). The analysis of LSBS in phosphate buffers at pH values between 7 and 9 indicates that the pH apparently has no effect on capsid assembly (data not shown). In Tris hydrochloride buffer (pH 8), 54% of all identified particles of wild-type LSBS are capsid-shaped; the other particles have irregular shape and are aggregated, deformed or incomplete (Figure 5(b)). The capsid-shaped particles appear in diameter ranges typical for type I (29%), type II/III (25%). At pH 9.0, only 49% of all detected particles have regular capsid-like shape (Figure 5(c)). The remaining particles have non-circular shape, which indicates deformation or an incomplete capsid shell. The regularly formed capsids belong to the type II/III category. In borate buffer (pH 7), LSBS forms both type I (80%) and type II/III capsids (20%) (Figure 5(d)). In phosphate buffer at pH 7.0, 89% of the LSBS Arg127Thr mutant particles have circular shape while a minor percentage of 11% have irregular shape. 75 % of the particles have circular shape with a diameter corresponding to type II/III capsids and

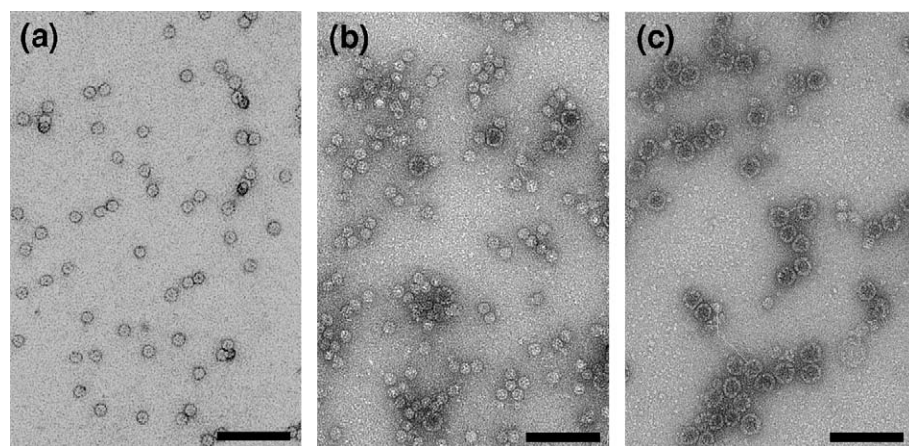


Figure 4. Electron micrographs of recombinant lumazine synthase from *B. subtilis* (a) and the mutants R127H (b) and R127T (c). The proteins were absorbed on carbon and negatively stained with uranyl acetate. The scale bar represents 100 nm.

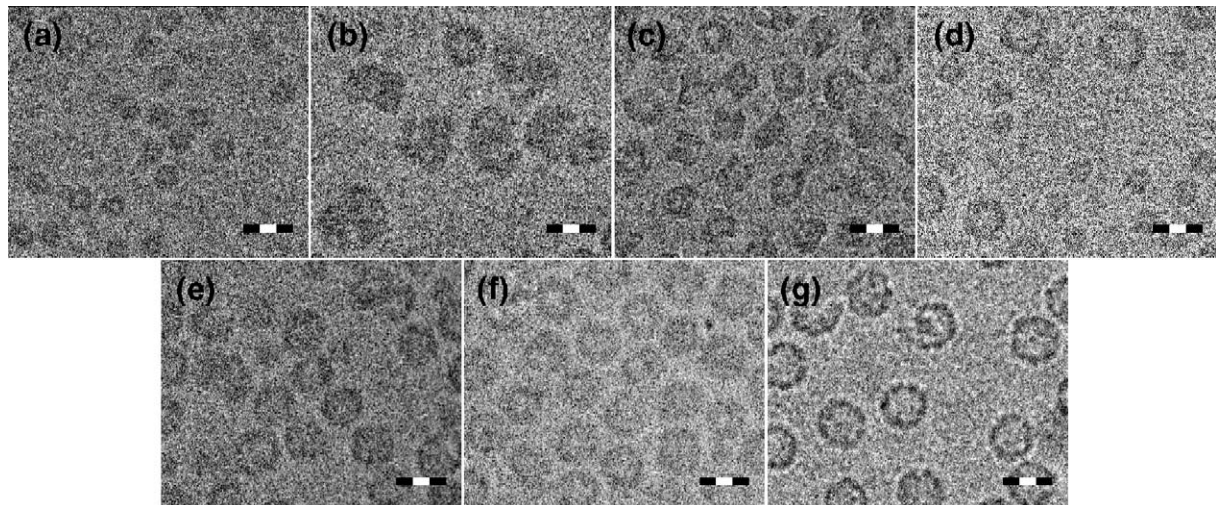


Figure 5. Contrast enhanced Cryo-EM micrographs of (a) LSBS phosphate (pH 8.0), (b) LSBS in Tris (pH 8.0), (c) LSBS in Tris-HCl (pH 9.0), (d) LSBS in borate (pH 7.0), (e) LSBS R127T mutant in phosphate (pH 7.0), (f) LSAQ-IDEA in Tris (pH 8.5), (g) LSAQ-IDEA in phosphate (pH 7.0). The scale bar represents 30 nm.

14 % of the particles correspond to type I capsids (Figure 5(e)). The remaining irregularly shaped particles have sizes comparable to either type I or type II/III. The LSAQ-IDEA mutant was found to exclusively assemble type II/III capsids in both Tris hydrochloride buffer (pH 8.5) (Figure 5(f)) and phosphate buffer (pH 7.0) (Figure 5(g)).

SAXS analysis of lumazine synthase wild-type and mutants

To systematically analyze the capsid assembly of LSBS/LSAQ, X-ray scattering experiments were performed with LSBS solutions in phosphate, Tris hydrochloride and borate buffers and with LSAQ solutions in phosphate and Tris hydrochloride buffers. The SAXS data from protein solutions and corresponding buffers were collected as described in Methods over a range of pH values between 6.0 and

10.0. Figure 6 presents the background corrected and processed scattering intensities as functions of momentum transfer $s=4\pi \sin(\theta)/\lambda$ (here, 2θ is the scattering angle and $\lambda=0.15$ nm is the X-ray wavelength) for LSBS and LSAQ, respectively. The overall parameters of the solutes (effective radius of gyration R_g , molecular weight M_w , as well as maximum particle size D_{max}) are summarized in Table 2.

The characteristic functions $p(r)$ computed from the experimental data by the indirect Fourier transformation program GNOM^{26,27} are displayed in Figure 7(a) to (c) (LSBS) and (d) (LSAQ). For monodisperse systems (e.g. for protein solutions containing one single species only), the overall parameters computed from the SAXS data correspond to this species. The characteristic function $p(r)$ is the distance distribution (averaged Patterson function) characterizing the shape of the particle, and this function goes to zero for $r > D_{max}$. For mixtures containing multiple species (components), the experimental scattering curve is a linear combination of the scattering from individual components weighted by their relative concentrations (i.e. their volume fractions in the solution). The effective values of R_g and M_w are also averages over the ensemble weighted by the volume fractions of the species, and the $p(r)$ functions of mixtures are weighted superpositions of the distance distributions of individual components, whereas D_{max} corresponds to the maximum distance of the largest particle in the mixture.

Up to three different types of capsids are assumed to be present in solutions of wild-type LS or their respective mutants. As in the section describing the results from EM studies we refer in the following text to capsids with an outer diameter of 160–200 Å as type I capsids, to capsids with a diameter of 270–300 Å as type II capsids and to capsids with a diameter of 300–330 Å as type III capsids. Type I capsids are

Table 1. Evaluation of particle populations by cryo-EM

Sample	Buffer	pH	Type I capsids (160–200 Å)	Type II/III capsids (270–330 Å)	Irregular particles
			Fraction size (%)	Fraction size (%)	Fraction size (%)
LSBS WT	Phosphate	8.0	100	-	-
LSBS WT	Tris-HCl	8.0	29	25 ^b	46 ^a
LSBS WT	Tris-HCl	9.0	-	49 ^b	51
LSBS WT	Borate	7.0	80	20 ^b	-
LSBS R127T	Phosphate	7.0	14	75 ^b	11
LSAQ IDEA	Tris-HCl	8.5	-	100 ^b	-

See Methods for a description of how particle sizes were evaluated.

^a A major fraction of the irregular particles observed in this sample are aggregates of intact capsids of different sizes.

^b The numbers in brackets indicate the percentages of particles smaller and larger than 300 Å.

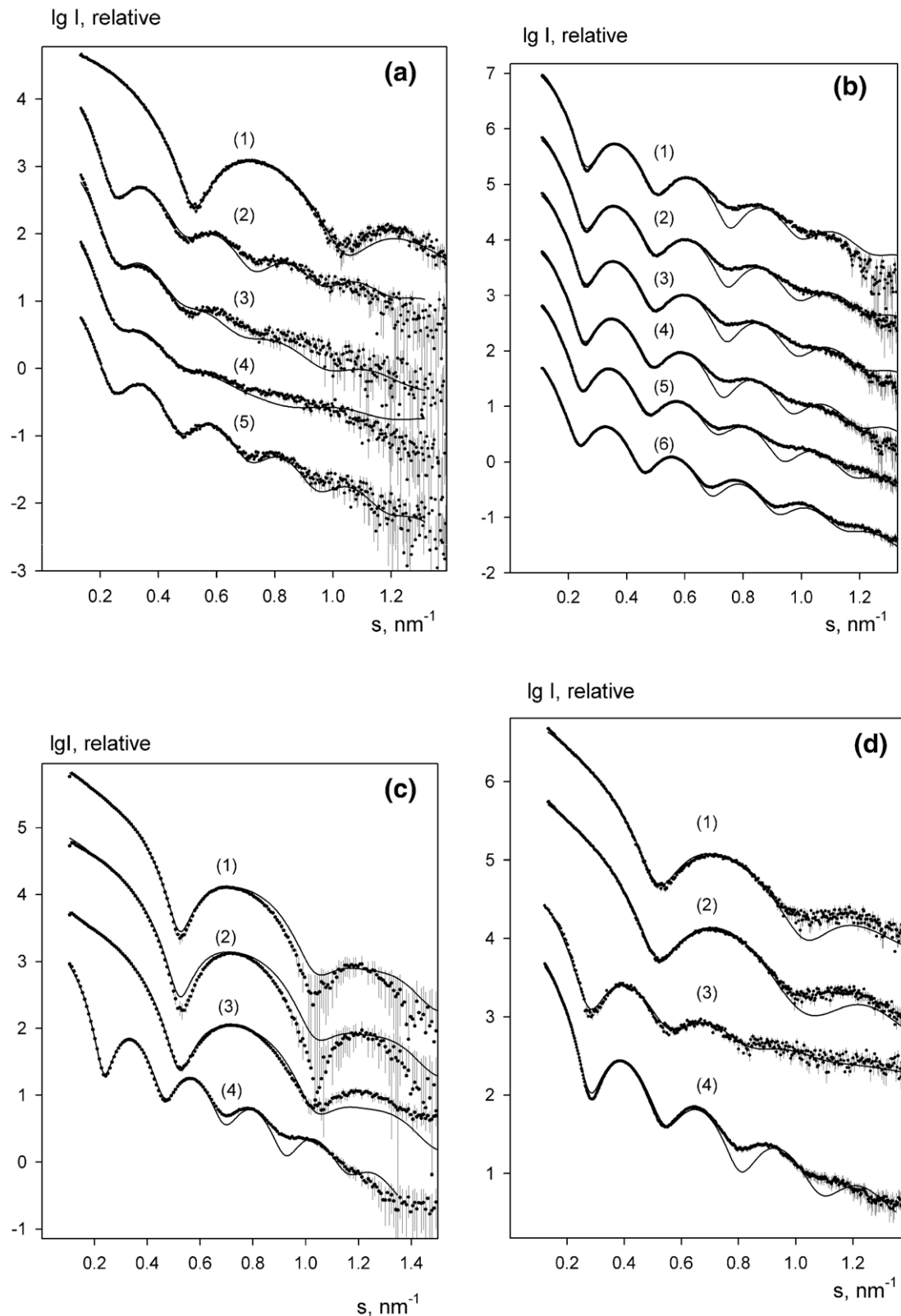


Figure 6. Experimental scattering curves of LSBS wild-type, LSBS R127 mutant, LSAQ wild-type and LSAQ-IDEA (circles) and fits (continuous lines) obtained from MIXTURE-M program. (a) LSBS wild-type: curve (1) corresponds to phosphate buffer at pH 6.0, curves (2)–(5) correspond to Tris hydrochloride buffer at pH 7.0, 7.6, 8.4 and 9.0, respectively. (b) LSBS R127 mutant: curve (1) corresponds to phosphate buffer at pH 6.0, curves (2) – (6) correspond to Tris hydrochloride buffer at pH 7.0, 7.5, 8.0, 8.5 and 9.0, respectively. (c) LSBS wild type: curves (1) – (4) correspond to borate buffer at pH=7.0, 8.0, 9.0 and 10.0, respectively. (d) Curve (1) corresponds to LSAQ wild-type in phosphate buffer at pH 6.0, curve (2) corresponds to LSAQ wild-type in Tris hydrochloride buffer at pH 7.0, curve (3) corresponds to LSAQ-IDEA in phosphate buffer at pH 6.0, curve (4) corresponds to LSAQ-IDEA in Tris hydrochloride at pH 7.0.

Table 2. Overall structural parameters of LS mixtures computed from the data

Enzyme	Buffers	pH	D_{\max} (nm)	M_{Wexp} (kDa)	R_{ge} (nm)
LSBS, wild-type	Phosphate, 0.1 M	6.0	30±2	595±50	6.9±0.2
		6.5	30±2	658±50	7.1±0.2
		7.0	30±2	607±50	7.3±0.2
		7.5	30±2	510±50	6.9±0.2
		8.0	30±2	581±50	7.1±0.2
	Tris-HCl, 0.1 M	7.0	32±2	856±70	12.8±0.3
		7.6	32±2	962±70	12.9±0.3
		8.4	32±2	936±70	12.8±0.3
		9.0	32±2	854±70	12.7±0.3
		10.0	31±2	1608±120	12.7±0.3
LSBS, wild-type	Borate, 0.1 M	7.0	16±1	1637±120	6.8±0.2
		8.0	16±1	1096±100	6.9±0.2
		9.0	16±1	814±70	6.8±0.2
		10.0	31±2	1608±120	12.7±0.3
		6.0	30±2	785±60	12.5±0.3
	Tris-HCl, 0.1 M	6.5	30±2	730±60	12.4±0.3
		7.0	30±2	683±50	12.6±0.3
		7.5	30±2	805±70	12.5±0.3
		8.0	30±2	752±60	12.4±0.3
		7.0	30±2	854±70	12.5±0.3
LSAQ, wild-type	Phosphate	7.5	31±2	661±50	12.7±0.3
		8.0	32±2	715±60	12.9±0.3
		8.5	32±2	644±50	13.1±0.3
		9.0	32±2	623±50	13.3±0.3
		6.0	32±2	806±70	10.0±0.3
	Tris-HCl	6.5	32±2	720±70	9.9±0.3
		7.0	32±2	687±60	9.8±0.3
		7.5	32±2	816±60	10.1±0.3
		8.0	32±2	855±60	10.0±0.3
		7.0	32±2	965±80	10.2±0.3
LSAQ- IDEA	Phosphate, 0.1 M	7.5	32±2	732±70	10.3±0.3
		8.0	32±2	772±70	9.8±0.3
		8.5	32±2	820±80	10.0±0.3
		9.0	32±2	678±70	8.8±0.2
		6.0	28±2	621±50	11.2±0.3
	Tris-HCl, 0.1 M	7.0	28±2	617±50	11.2±0.3
		8.0	28±2	888±70	11.1±0.3
		7.0	28±2	683±60	11.3±0.3
		7.5	28±2	949±80	11.2±0.3
		8.0	28±2	1182±100	11.2±0.3

D_{\max} , M_{Wexp} , R_{ge} , are the maximum size, the molecular mass and the radius of gyration calculated from the scattering data (for mixtures, the values M_{Wexp} and R_{ge} correspond to the average over the ensemble).

constituted by 60 subunits with perfect icosahedral symmetry ($T=1$) as has been shown by X-ray crystallographic methods. The molecular structure of type II and type III capsids is so far unknown, however, our attempts to model the observed data indicate that the respective diameters of idealized capsids following the triangular numbers $T=3$ or $T=4$ match the diameters of type II and type III capsids as observed in the described SAXS experiments (Figure 8). The diameters of real $T=3$ or $T=4$ capsids may be considerably different from the ones of the models shown in Figure 8(b) and (c). The capsid diameters could for instance further decrease, if some subunits would be partially buried by others. On the other hand, a cage-like assembly could lead to a more expanded capsid. Type III particles may therefore even correspond to an expanded $T=3$ form.

For capsid shaped particles the maximum size is equivalent to the outer capsid diameter and the shape of the $p(r)$ function permits qualitative conclusions about the composition of the mixtures in different buffers at different pH values. Thus, wild-type LSBS consistently forms small (type I) capsids in phosphate (Figure 7(a), curve 1) but large (type III) capsids in Tris buffer (Figure 7(a), curves 2–5). In borate buffer, a transition is observed from type I (pH from 7.0 to 9.0) to type III capsids at pH 10.0 (Figure 7(c)). The wild-type LSAQ solutions (Figure 7(d), curves 1–2) contain mainly small capsids, although the larger particles are also present. At the same time, larger capsids are predominant in the mutants LSBS R127T (Figure 7(b)) and LSAQ-IDEA (Figure 7(d), curves 3 and 4) solutions at all conditions studied.

The $p(r)$ function of LSBS in phosphate does not significantly depend on pH. The curves indicate capsids with an outer diameter of about 160 Å, which is in line with the size of the icosahedral $T=1$ capsid observed in the crystal, and a small amount of larger particles (yielding a small contribution of interparticle distances from 160 to 330 Å in Figure 7(a), curve 1). In contrast, the distance distribution curves of LSBS in Tris hydrochloride (Figure 7(a), curves 2–5) point out the presence of large capsids with an outer diameter of about 320 Å. Interestingly, the curves at pH 7.0 and 9.0 display pronounced maxima suggesting rather isometric particle shapes, whereas in those at pH 7.6 and 8.4 the maxima appear smeared, indicating possible polydispersity or deformation of the particles. One can conclude that a structural transition is taking place in Tris at around pH 8.0.

The $p(r)$ function of the LSBS R127T mutant in phosphate (Figure 7(b), curve 1) indicates largely capsids with an outer diameter of about 300 Å and this mutant does not reveal dependence on pH. In contrast, the distance distribution curves of the LSBS R127T mutant in Tris hydrochloride buffers (Figure 7(b), curves 2–6) vary considerably with pH. At pH 7.0 the $p(r)$ is similar to that of LSBS R127T in phosphate buffer (corresponding to type III particles), but at higher pHs yet larger particles appear with diameter of about 320–330 Å (which corresponds to larger type III particles). In borate buffer (Figure 7(c)) LSBS displays a similar but even more pronounced dependence of the capsid formation on pH as in Tris hydrochloride. At pH values (7.0, 8.0 and 9.0) mainly small particles (type I) are present (Figure 7(c), curves 1–3) whereas at pH 10.0, mostly large particles (type III) are formed (Figure 7(c), curve 4).

The scattering patterns and distance distribution functions of LSAQ in phosphate and Tris hydrochloride buffers are very similar to each other and they display practically no pH dependence (Figure 7(d), curves 1 and 2). Here, the main maximum of the profile of $p(r)$ corresponds to the small type I particles although a noticeable amount of larger particles are present. Rather different results were obtained for the LSAQ-IDEA mutant prepared as

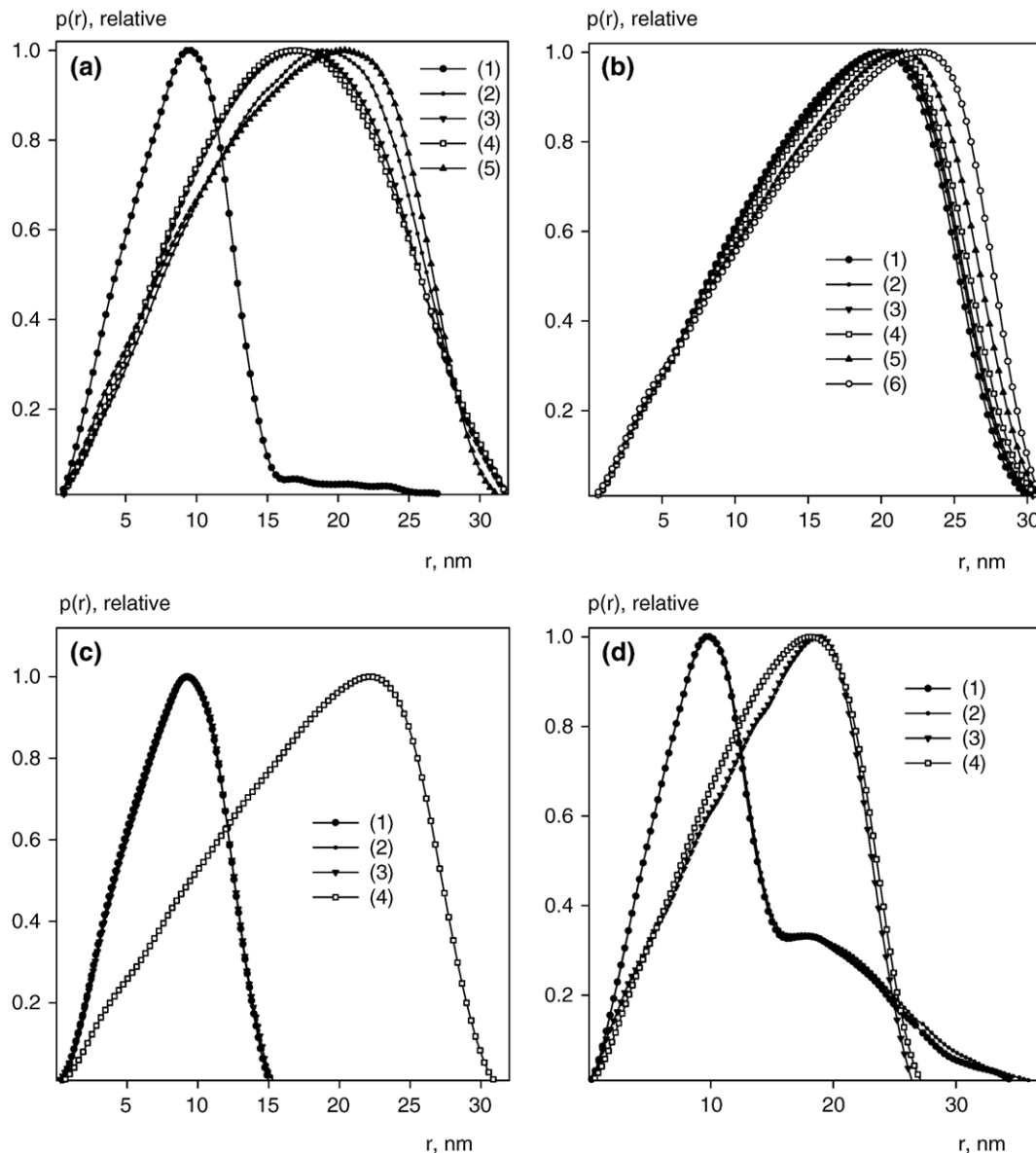


Figure 7. Distance distribution functions $p(r)$ of (a) LSBS wild-type in phosphate and Tris (curve (1) corresponds to phosphate buffer at pH 6.0, curves (2) – (5) correspond to Tris hydrochloride buffer at pH 7.0, 7.6, 8.4 and 9.0, respectively); (b) LSBS R127 mutant in phosphate and Tris (curve (1) corresponds to phosphate buffer at pH 6.0, curves (2) – (6) correspond to Tris hydrochloride buffer at pH 7.0, 7.5, 8.0, 8.5 and 9.0, respectively); (c) LSBS wild-type in borate (curves (1) – (4) correspond to pH 7.0, 8.0, 9.0, and 10.0, respectively); (d) LSAQ wild-type (curve (1), wild-type enzyme in phosphate buffer at pH 6.0; curve (2), wild-type enzyme in Tris hydrochloride buffer at pH 7.0; curve (3), LSAQ-IDEA mutant in phosphate buffer at pH 6.0; curve (4), LSAQ-IDEA mutant in Tris hydrochloride at pH 7.0). All distance distribution functions are normalized to the maximum value of unity.

described in Methods to test the hypothesis that the four residues insert between helix α_4 and helix α_5 prevents the formation of a capsid and instead leads to pentameric assemblies. Kinetic studies of the LSAQ-IDEA mutant revealed less than 0.5% activity with respect to the wild-type enzyme. Surprisingly, instead of pentamers, the LSAQ-IDEA mutant was found to form rather large particles in both phosphate and Tris hydrochloride buffer. The scattering curves in the two buffers are similar to each other and show little dependence on pH (Figure 6(d), curves 3 and 4), and the calculated p

(r) functions (Figure 7(d), curves 3 and 4) point to the presence of hollow capsids with D_{\max} about 275 Å (type II capsids), which is larger than T1 (type I), but smaller than the diameters of the largest particles (300–320 Å, type III) formed by the R127T mutant of LSBS.

The above analysis of the $p(r)$ functions indicates that both LSBS and LSAQ-IDEA solutions are mixtures of particles of different size. The scattering curves displaying sharp minima suggest that the particles are rather isometric, whereas the profiles of the $p(r)$ functions in the cases where one particle

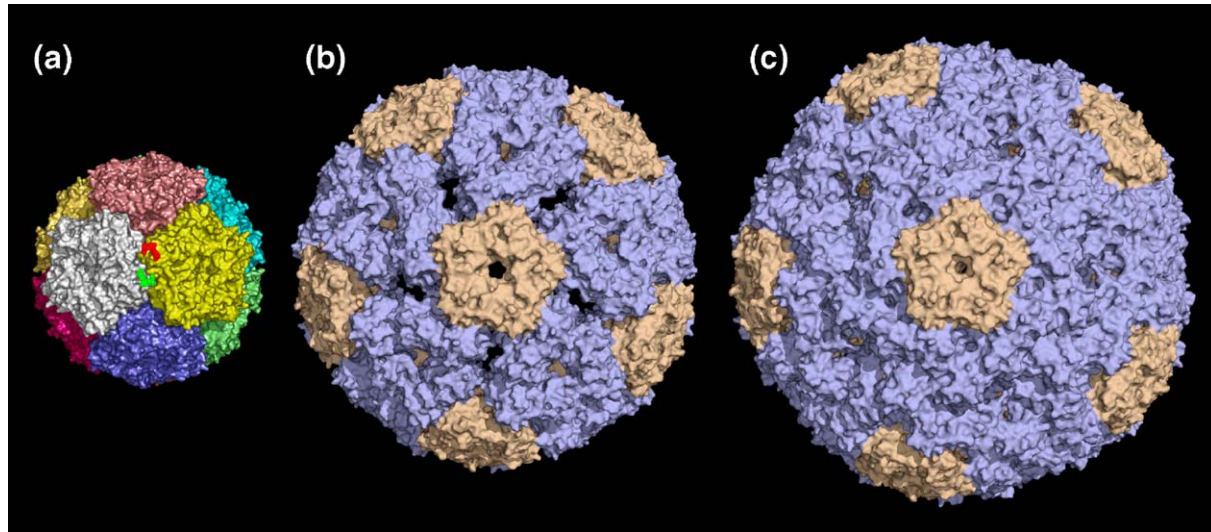


Figure 8. Surface representations of (a) the crystal structure of the $T=1$ LSAQ-WT capsid with a diameter of 160 Å (the residues Arg127, Ala128, Gly129, and Thr130 of the pentameric blocks forming the central inter-pentamer interface are shown as overlay and are marked in red and green color, respectively; these residues are located at the inner surface of the capsid close to the pentamer–pentamer interface); (b) a model of a $T=3$ icosahedral capsid with a diameter of ~290 Å; (c) a model of a $T=4$ icosahedral capsid with a diameter of ~320 Å. The models of the $T=3$ and $T=4$ capsids were produced based on icosahedral geometry and the crystal structure of the $T=1$ capsid, from which the subunit contacts were adopted and fine adjusted in order to generate a proper curvature. The subunits were placed at the same distance to the capsid center. All representations are on the same scale.

type is dominating (e.g. curve 1 in Figure 7(a), curves 4 in Figure 7(c) and (d)) showing a steep decrease when $p(r)$ approaches D_{\max} are typical for hollow particles. These data suggest that the solutions contain rather isometric hollow particles. To further assess the particle shapes and check whether these particles are ideally icosahedral a version of an *ab initio* program DAMMIN accounting for icosahedral symmetry (see Methods) was used to reconstruct the shapes of LSBS particles in borate buffer at pH 7 and pH 10, expected to predominantly contain type I and type III capsids, respectively. The two reconstructions (Figure 9, models (a) and (c)) appear rather similar to the type I and type III models, but the computed patterns display systematic deviations from the experimental data (Figure 10). The minima in the model curves from icosahedral structures appear sharper than those in the experimentally observed data. This indicates that the models are apparently too isometric. To verify this, the icosahedral models in Figure 9(a) and (c) were further refined against the experimental data by omitting the symmetry restriction. The resulting models, also presented in Figure 9(b) and (d), neatly fit the experimental data (Figure 10) and appear like hollow icosahedral particles with missing facets, which are similar in size to a pentameric building block of a $T=1$ capsid. Similar results were obtained from the scattering data from other samples, suggesting that the LS assemblies may contain significant proportions of incomplete icosahedral particles with some of the facets missing in the structure. Interestingly, type I particles (model (b)) appear more isometric (possibly, having less material missing) than type III particles (model (d)).

Several attempts were made to fit the experimental data from LS solutions by the scattering patterns computed from the high-resolution models. The fitting by single species, either full icosahedral capsids or those with (one or several) missing facets did not yield reasonable agreement to the data. It was therefore assumed that type I and type II or III capsids may co-exist, so that the data have to be fitted by scattering from mixtures of several components. Taking into account the presence of incomplete capsids revealed by *ab initio* modeling, the five components were found to adequately represent the system: (1–2) complete and incomplete type II or type III capsid; (3–4) complete and incomplete type I capsid; (5) smaller capsid substructures of the type I capsid. The incomplete type I and type II or III capsids were lacking one and two facets, respectively. To take possible variation in sizes and type I to type II or III transition into account, polydispersity of the complete and incomplete capsids was introduced. For this, the scattering from the type I and type II/III capsids was computed as “basic” form-factors. The scattering from type I and type II/III particles with a diameter d could then be represented by rescaling these form-factors $I(s,d)=(d/d_0)^3 I(s^*d_0/d)$, where d_0 is the nominal diameter. This parameter was $d_0=160$ Å for type I and 290 Å for large capsids, which could be either type II (for $d < 280$ Å) or type III (for $d > 300$ Å particles). Using this approach, Gaussian size distribution of the components was incorporated into the program MIXTURE-M fitting the experimental data by linear combination of the scattering from the five components to find their volume fractions and polydispersity

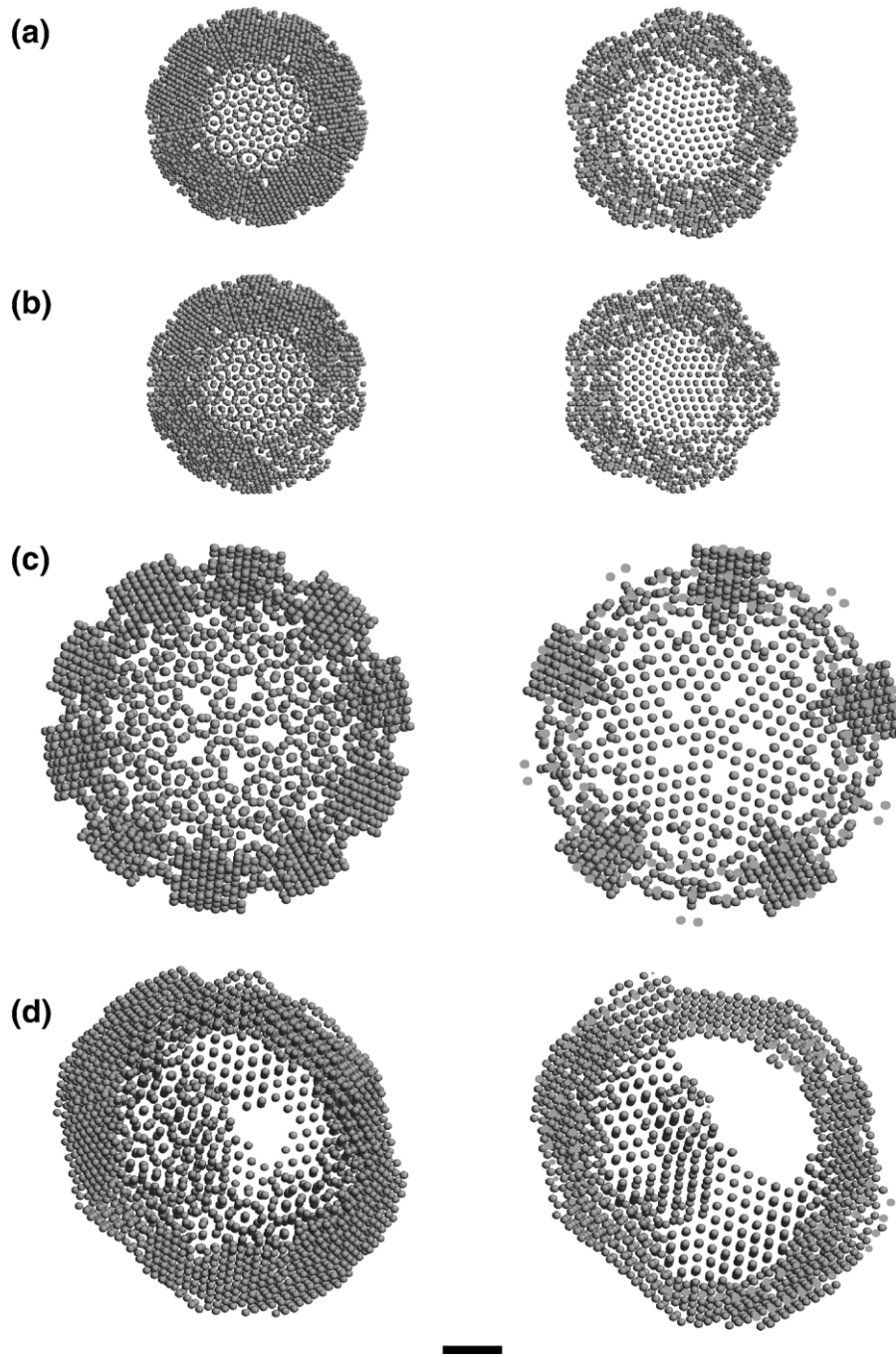


Figure 9. Typical low-resolution models of LSBS in borate buffer at pH 7 ((a) and (b)) and pH 10 ((c) and (d)) restored *ab initio* by DAMMIN program. Models (a) and (c) were obtained under icosahedral symmetry restrictions, whereas models (b) and (d) have $P1$ symmetry. The models were displayed using the program RASMOL³⁹ in space filling (left side) and slab (right side) modes. The scale bar represents 2 nm.

(see Methods). The average radii of the components 1–4 were allowed to vary around the corresponding d_0 values, whereas their polydispersity (width of the Gaussian distribution) was restricted not to exceed 5 Å for complete capsids, but could reach up to 30 Å for the incomplete capsids type I and type II/III.

It should be noted here, that the selection of smaller capsid substructures as the additional component was made to some extent arbitrarily

but the results were not significantly dependent on the specific choice of the form factor representing the small particles in solution as long as these particles were small compared to the capsids. An alternative approach was also tested assuming that the deviations from the icosahedral symmetry are not due to the lacking facets but rather due to deformations of the capsids. It was found that affine deformations of the ideal icosahedral particles up to 15–20% were required to smear the

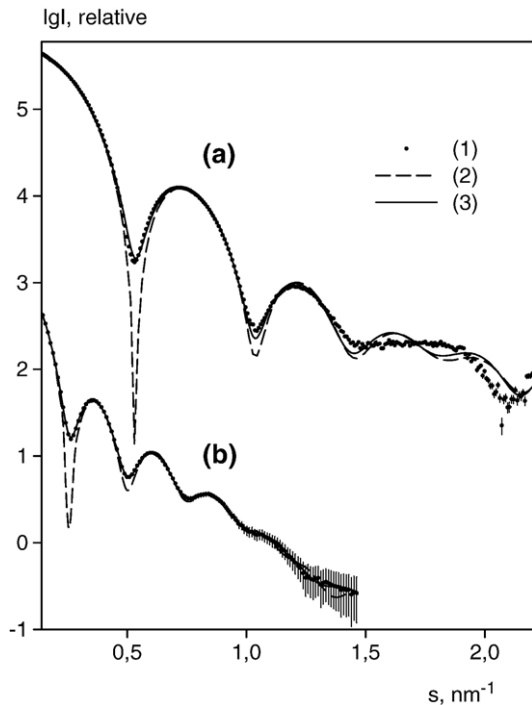


Figure 10. Experimental scattering curves of LSBS in borate buffer (filled spheres) and the fits obtained from *ab initio* DAMMIN modeling with icosahedral symmetry restrictions (broken curves) and without symmetry restrictions (continuous curves). (a) Corresponds to the buffer pH of 7.0, whereas (b) to pH of 10.0.

minima in the computed data, but even these very large deformations yielded fits that were worse than those from the models with the missing facets. Given also that the *ab initio* models pointed to missing facets but not to deformed particles, the latter hypothesis was found to be less compatible with the experimental data.

The results of the fitting procedure are summarized in Table 3 and the fits are presented in Figure 6. Overall, the five-component model affords a reasonably good fit to the experimental data.

For wild-type LSBS in phosphate buffer, three components were found: complete type I capsids (varying from 85% to 90% of volume fraction), free facets (volume fractions from 6% to 13%), and complete type II capsids (volume fraction from 1% to 3%). The sizes of type I and type II capsids are close to the theoretical values of 160 \AA and 270 \AA , correspondingly. In contrast, for wild-type LSBS in Tris buffer there is a significant volume fraction of large type III capsids (from 45% to 76%) with the outer diameter in the range from 290 to 310 \AA . Also, strong pH dependence is observed, whereby at pH 7.0 and 9.0 the dominating fractions are from large capsids, while at pH 7.6 and 8.4 a significant amount (from 30% to 45%) of small (type I) capsids is found. The smeared maxima at pH 7.6 and 8.4 were poorly fitted by the model, which may point e.g. to the presence of deformed particles in solution during this transition.

The LSBS R127T mutant forms three different components in phosphate and Tris buffer, which correspond to the form factors of complete type III capsids (75–80% volume fraction), incomplete type III capsids (16–21% volume fraction) and incomplete type I capsids (4% volume fraction). A relatively high degree of polydispersity (from 10 to 20 \AA) is observed for the incomplete structures. It should be stressed that for the LSBS R127T mutant in phosphate buffer the volume fractions and the size of the components do not depend on pH, whereas for LSBS R127T in Tris buffer there is strong pH dependence. The average size of type III component is increasing with pH (from 300 \AA at pH 7 to 330 \AA at pH 9). This can be explained by the structural transition of type III icosahedral capsids between pH 7 and 9.

The results for LSBS in borate buffer strongly depend on pH. At pH values of 7, 8, and 9, mainly type I capsids are formed (volume fraction 97%) with diameters of about 160 \AA , whereas at pH 10.0 the main fraction (62% complete and 36% incomplete capsids) belongs to type III capsids with diameters of about 320 \AA . These results reveal a strong dependence of the formation of icosahedral LSBS capsids in borate buffer on pH value. This means that the process of capsid formation can be tuned by pH of the buffer solution and the multiple ensembles of different types of capsids are in equilibrium.

For wild-type LSAQ in phosphate and Tris buffer, three components were found: 10–18% of free facets, 61–70% of complete type I capsids with the diameter of 155 – 160 \AA and 20–22% of complete type II capsids with the diameter of 260 – 270 \AA . The insertion of four residues in the LSAQ-IDEA construct leads to substantial changes in the scattering profile (Figure 6(d)). The type I component practically disappears (only up to 5% of these particles were found); instead there are mainly type II capsids with the diameter of 270 \AA and a small amount of small capsid substructures. These results indicate that the IDEA mutation prevents formation of type I capsids but not of type II capsids.

Conditions triggering dissociation and association of lumazine synthase capsids

Some viral proteins can assemble capsids of varying size and number of subunits as a consequence of mutations or changes of the chemical and physical environment (for a review see Rossmann & Erickson).²⁸ A number of biochemical and structural studies published previously and presented here suggest that LS exhibits such structural variability, as well. This variability is correlated with residues in the active site and thus with the function of the enzyme.

As shown by two independent methods, both LSBS and LSAQ wild-type protein and mutants are to different extent capable of forming type I capsids and larger capsids with presumably icosahedral symmetry. However, the conditions leading to

Table 3. Structural parameters of LS mixtures

Enzyme	pH	χ	Small capsids						Large capsids						Free facets			
			Complete			Incomplete			Complete			Incomplete			Free facets			
			v	R (nm)	dR (nm)	V	R (nm)	dR (nm)	v	R (nm)	dR (nm)	v	R (nm)	dR (nm)	v	R (nm)	dR (nm)	
LSBS	6.0	1.08	0.912	7.83	0.4	0.0	—	—	0.022	13.47	0.5	0.0	—	—	0.065	3.0	0.2	
WT	6.5	1.10	0.907	7.85	0.4	0.0	—	—	0.019	13.42	0.5	0.0	—	—	0.074	3.0	0.2	
(Ph)	7.0	1.02	0.887	7.86	0.3	0.0	—	—	0.032	13.43	0.5	0.0	—	—	0.081	3.0	0.3	
	7.5	1.30	0.863	7.89	0.2	0.0	—	—	0.015	13.48	0.2	0.0	—	—	0.122	3.0	0.2	
	8.0	1.43	0.849	7.90	0.3	0.0	—	—	0.014	13.84	0.1	0.0	—	—	0.135	3.0	0.3	
LSBS	7.0	1.51	0.161	9.00	0.3	0.0	—	—	0.762	15.11	0.5	0.0	—	—	0.077	3.0	0.3	
WT	7.6	2.57	0.305	9.00	0.5	0.0	—	—	0.633	14.52	0.5	0.0	—	—	0.062	3.0	0.3	
(Tris)	8.4	2.27	0.455	9.00	0.4	0.0	—	—	0.454	14.67	0.5	0.0	—	—	0.091	3.0	0.2	
	9.0	1.09	0.104	9.00	0.3	0.0	—	—	0.573	15.52	0.5	0.0	—	—	0.323	3.0	0.2	
LSBS	7.0	1.28	0.97	7.69	0.50	0.0	—	—	0.02	15.72	0.5	0.01	14.77	0.27	0.0	—	—	
WT	8.0	2.47	0.96	7.72	0.50	0.0	—	—	0.02	15.64	0.5	0.01	14.65	0.24	0.0	—	—	
(Borate)	9.0	2.81	0.98	7.54	0.50	0.0	—	—	0.01	15.95	0.5	0.01	14.72	0.15	0.0	—	—	
	10.0	3.72	0.02	9.00	0.10	0.0	—	—	0.62	15.92	0.5	0.36	12.94	0.99	0.0	—	—	
LSBS	6.0	5.41	0.0	—	—	0.04	9.00	1.27	0.80	14.70	0.5	0.16	11.70	0.10	0.0	—	—	
R127	6.5	6.71	0.0	—	—	0.03	9.00	1.34	0.79	14.73	0.5	0.18	11.73	0.10	0.0	—	—	
Mutant	7.0	7.25	0.0	—	—	0.03	9.00	1.19	0.79	14.76	0.5	0.18	11.75	0.10	0.0	—	—	
(Ph)	7.5	2.98	0.0	—	—	0.03	9.00	1.52	0.75	14.83	0.5	0.22	11.81	0.10	0.0	—	—	
	8.0	2.78	0.0	—	—	0.04	9.00	1.47	0.75	14.92	0.5	0.21	11.98	0.10	0.0	—	—	
LSBS	7.0	4.62	0.0	—	—	0.05	9.00	1.33	0.75	14.87	0.5	0.20	11.87	0.10	0.0	—	—	
R127	7.5	4.91	0.0	—	—	0.04	9.00	1.25	0.74	14.96	0.5	0.22	11.93	0.10	0.0	—	—	
Mutant	8.0	4.60	0.0	—	—	0.04	9.00	1.13	0.70	15.22	0.5	0.26	12.24	0.10	0.0	—	—	
(Tris)	8.5	3.30	0.0	—	—	0.03	9.00	1.23	0.54	15.76	0.5	0.43	12.77	0.10	0.0	—	—	
	9.0	5.66	0.0	—	—	0.03	9.00	1.19	0.47	16.27	0.5	0.50	13.24	0.10	0.0	—	—	
LSAQ	6.0	2.37	0.62	7.95	0.5	0.0	—	—	0.21	13.11	0.5	0.0	—	—	0.17	3.0	0.1	
WT	6.5	2.06	0.65	7.92	0.5	0.0	—	—	0.21	13.15	0.5	0.0	—	—	0.14	3.0	0.1	
(Ph)	7.0	2.05	0.62	7.93	0.5	0.0	—	—	0.23	13.23	0.5	0.0	—	—	0.15	3.0	0.1	
	7.5	2.08	0.64	7.94	0.5	0.0	—	—	0.22	13.12	0.5	0.0	—	—	0.14	3.0	0.1	
	8.0	1.96	0.61	7.98	0.5	0.0	—	—	0.23	13.34	0.5	0.0	—	—	0.16	3.0	0.1	
LSAQ	7.0	2.47	0.63	7.98	0.5	0.0	—	—	0.19	14.50	0.5	0.0	—	—	0.18	3.0	0.1	
WT	7.5	1.70	0.69	7.95	0.5	0.0	—	—	0.21	14.56	0.5	0.0	—	—	0.10	3.0	0.1	
(Tris)	8.0	1.99	0.69	7.94	0.5	0.0	—	—	0.18	14.58	0.5	0.0	—	—	0.13	3.0	0.1	
	8.5	1.86	0.68	7.93	0.5	0.0	—	—	0.20	14.52	0.5	0.0	—	—	0.12	3.0	0.1	
	9.0	2.12	0.67	7.95	0.5	0.0	—	—	0.17	14.51	0.5	0.0	—	—	0.16	3.0	0.1	
LSAQ	6.0	2.38	0.0	—	—	0.01	9.00	0.1	0.67	13.41	0.5	0.0	—	—	0.32	3.0	0.1	
IDEA	7.0	2.09	0.0	—	—	0.02	9.00	0.1	0.81	13.29	0.5	0.0	—	—	0.17	3.0	0.1	
(Ph)	8.0	2.21	0.0	—	—	0.01	9.00	0.1	0.77	13.55	0.5	0.0	—	—	0.22	3.0	0.1	
LSAQ	7.0	3.75	0.0	—	—	0.05	9.00	0.1	0.95	13.73	0.5	0.0	—	—	0.0	—	—	
IDEA	7.5	2.47	0.0	—	—	0.04	9.00	0.1	0.96	13.73	0.5	0.0	—	—	0.0	—	—	
(Tris)	8.0	2.61	0.0	—	—	0.05	9.00	0.1	0.95	13.74	0.5	0.0	—	—	0.0	—	—	
	8.5	2.13	0.0	—	—	0.03	9.00	0.1	0.97	13.76	0.5	0.0	—	—	0.0	—	—	
	9.0	2.17	0.0	—	—	0.04	9.00	0.1	0.96	13.82	0.5	0.0	—	—	0.0	—	—	

χ is the discrepancy between the experimental data and scattering curves calculated from the mixture composition of the high-resolution models as provided by the program MIXTURE-M, with the given volume fractions of the components (v), their average size (R) and degree of polydispersity (dR). For the abbreviations of the components, see the text.

multiple assembly states are different. LSBS assembles mainly the type I capsids in phosphate buffers at all pH values. In Tris hydrochloride and borate buffers, the enzyme forms large aggregates to a varying extent (Table 3 and Figure 5). LSAQ associates to capsids of different sizes in both phosphate and Tris hydrochloride buffers at all pH values. Remarkably, at many conditions the different forms of LS co-exist and are presumably related *via* equilibrium, which is fine-tuned by pH or the presence of specific ions. The tendency of large capsid formation is overruled by mutation of residues in or close to the active site as well as the insertion of four residues in the LSAQ-IDEA construct. Thus, the results from small angle scattering experiments and electron micrographs indicate that multiple assembly states are a general

feature of native and mutant icosahedral lumazine synthases.

The LSAQ-IDEA mutant is unable to form a type I capsid as anticipated by the fact that at the position of the IDEA-insertion, two adjacent pentamers within a type I model would severely clash. Instead of pentamers the mutant forms mostly type II capsids with a diameter of 270 Å (Table 3). The catalytic activity of this mutant is reduced to less than 0.5%. Although the native LSSC contains the IDEA insert at the corresponding position in the sequence, the conformational differences in the active site region of LSSC and the icosahedral LSBS are only minor.¹² This suggests that the insertion of the four residues IDEA in the LSAQ sequence does not necessarily by itself lead to local conformational changes of active site residues. The

loss of enzymatic activity could rather be due to the rearrangement of interpentameric interfaces, which would also affect the interfaces between neighboring subunits of the same pentamer.

The active sites of lumazine synthases are formed by two adjacent subunits; the catalytic activity of the enzyme is therefore dependent on an intact interface of two subunits belonging to the same pentamer unit. A relative shift of adjacent subunits forming the active site, which is likely to take place during the transformation to larger capsids, will also disrupt the substrate-binding site and thus deactivate the enzyme. There is so far no information about the molecular structure of large LS capsids at high resolution. However, preliminary experimental data suggest the formation of icosahedral capsids consisting of 180 subunits.¹⁹ Most likely, at least a majority of subunit pairs would not form interfaces between subunits that would reconstitute proper substrate binding pockets. Due to potential conformational changes of the active site, the larger capsids would be unable to carry out the catalytic functions of a functional $T=1$ capsid. Likewise, the formation of larger capsids triggers a change of the capsid curvature, which could lead to the perturbation of active sites that are located between adjacent subunits within one pentamer. Due to the interruption of a proper subunit interface the substrate-binding sites in large LS capsids would have a different conformation compared to those in the $T=1$ capsids. The observed residual activity of the mutants, which assemble capsids of different sizes, might be due to the presence of $T=1$ capsids.

Because the active site of icosahedral lumazine synthases is located close to the inner wall of the capsids, which implies that the free passage to the solvent is obstructed by the capsid wall, the substrate and product transfer has been of great interest and discussed extensively during the past decades.^{11,24,29} From a structural point of view, the 5-fold channels of the $T=1$ capsids could potentially serve as the diffusion pathway.⁸ However, the available high-resolution structures indicate that the 5-fold channels do not seem wide enough to allow riboflavin, the product of the reaction catalyzed by the enclosed riboflavin synthase, to pass through. Furthermore, incubation with $[\text{NaP}_5\text{W}_{30}\text{O}_{110}]^{14-}$, which is known to block the 5-fold channels of heavy riboflavin synthase from *B. subtilis*, did not result in a decreased enzymatic activity.²⁴ Alternative channels close to the 2-fold and 3-fold axes might allow the diffusion of LS substrates and products, but might be too narrow for riboflavin. This implies that the transfer of substrates and product could follow another mechanism. An icosahedral LS with a larger number of subunits will most likely be less densely packed and allow for easier access to the binding sites.

The exact effect of the described mutations is not well understood, the observations can however be interpreted such that a destabilization of both intra-

and inter-pentamer interfaces alleviates and triggers the formation of large capsids. Large capsids would thus be thermodynamically favored unless specific interactions at the subunit interface, in particular the active site would prevent them from being formed.

A model relating catalysis and subunit rearrangements

In recent studies, an expanded conformation of the pentameric building blocks in both the wild-type LS from *B. subtilis* (L. X. et al., unpublished results) and the LSAQ-IDEA mutant (L. Nilsson et al., unpublished results) has been observed. Based on observations presented earlier and here, we suggest here a mechanism that relates catalytic function and mode of assembly and suggest a model for the substrate and product transfer.

As shown earlier in a comparative study, the reaction is likely to proceed without rearrangement of the binding site.²¹ There is no experimental evidence whether the eliminated phosphate ion would keep being attached to Arg127 during the reaction or at least transiently be removed from the phosphate-binding site. However we proposed in a previous article, that the substrate (b) is moved away from the phosphate-binding site, whereupon a phosphate group is eliminated from substrate (b). In the subsequent step it might either bind back to the phosphate-binding site or leave the active site.²¹ The results and considerations presented here indicate that the formation of proper subunit contacts critically depends on the presence of phosphate or a ligand in the active site and the correct alignment of residue contacts spanning the interface. The absence of these stabilizing contacts, for instance the release of the inorganic phosphate ion from the binding site, could thus destabilize the $T=1$ capsids. This destabilization, which may eventually lead to the large capsid, might be thermodynamically driven.

Upon conclusion of the reaction the substrate-binding site could open up or even be disrupted. The formation of a large capsid requires a substantial extent of subunit rearrangements, which probably do not proceed on the same time scale as the reaction. It is therefore unlikely that the enzyme would form larger capsids during the catalytic cycle. However, the disruption of the active site might be driven by similar forces as the formation of large capsids and eventually lead to a similar local conformation of the pentamer building block. When the binding site is disrupted, the enzyme is not capable of catalysis anymore. This new state might also provide a local opening of the pentamer units, and therefore allows for easier passage of substrates and products through the capsid wall. Pentamer blocks with a widened opening around the 5-fold axis have been observed in low-resolution structures of both the wild-type LSBS capsid and the LSAQ-IDEA mutant (L. X. et al., unpublished results).

As observed by Bacher *et al.*, large capsids are readily converted to $T=1$ capsids after treatment with a substrate analogue.¹⁹ We therefore conclude that in the process of substrate binding, the opened and unfunctional binding site rearranges back to the functional state and is thus available to a new catalytic cycle. The rearrangement of LS during the reaction cycle might have a biological and physiological meaning: it has evolved to throttle the catalytic process, in this way keeping the concentration levels of lumazine and riboflavin low in the cell.

Methods

Molecular biological and enzymological methods

The wild-type LS from *B. subtilis* and *A. aeolicus* were prepared by published procedures.^{13,30} The mutants LSBS Arg127Thr and LSAQ-IDEA were prepared as described elsewhere (L. Nilsson, unpublished).²⁰ In the LSAQ-IDEA mutant the residues Ile, Asp, Glu and Ala are inserted after residue Gly129.

Electron microscopy

The protein solutions used for electron microscopic studies contained about 1 mg protein/ml and 20 mM potassium phosphate (pH 7.0). Carbon-coated copper grids were exposed to a glow discharge. They were covered with a drop of protein solution for 2 min and rinsed repeatedly with 2% uranyl acetate and distilled water. They were finally soaked with 2% uranyl acetate for 90 s and blotted dry with filter paper. Electron micrographs were obtained with a JEOL-JEM-100CX Microscope on Imago-EM 23 electron microscopy films.

The cryo-EM studies were performed according to the procedure described.³¹ Briefly, 3 μ l of LS solution was applied on a glow discharged EM grid coated with holy carbon film. After removal of excess solution with filter paper blotting, the EM grid was rapidly plunged into liquid ethane cooled by liquid nitrogen. The LS sample was thus quickly frozen in a thin layer of vitrified ice. The specimen was transferred into a FEI CM120 electron microscope with Gatan 626 cryo-transferring system and observed with desired magnification under a LaB6 filament operated at 120 kV. The focal pair images were recorded on Kodak SO163 electron sensitive film, with $-1 \mu\text{m}$ defocus for the first exposure and $-3 \mu\text{m}$ defocus for the second exposure.

The images with a clear particle profile and free of stigmatism were selected and digitized using a Heidelberg SCAN scanner with a step size of 7 μm , 10 μm or 14 μm . The pixel sizes were determined from the step size and the EM magnification. After digitization, the individual particle projections were sorted out from the images.

In order to evaluate the size distributions of the particles in the sample, areas on the raw images with representative particle distributions with at least 100 particles were selected. The particles were manually fitted into circles with diameters corresponding to 140, 200 \AA , 275 \AA , 305 \AA and 335 \AA . The circle diameter was stepwise increased and particles, whose projected area fitted into the respective circle area were marked. Particles with well-defined spherical shape and relatively

clear boundary were counted as complete capsids. Particles with non-spherical shapes were regarded as irregular particles. In the sample of wild-type LSBS in Tris hydrochloride (pH 8.0), most irregular particles look like aggregates of complete capsids with different sizes. Due to the sensitivity limit, aggregates with a size smaller than 150 \AA , e.g. free facets or small fractions of capsids observed by the SAXS experiments, could not be unambiguously identified and were therefore excluded from this analysis.

SAXS data collection and evaluation

Protein samples were prepared by buffer exchange using a Heraeus Biofuge 22 R centrifuge (6000 rpm) and Microsep membrane filters (30 kDa cutoff). The protein stock solutions were diluted tenfold in new buffers before centrifugation. The dilution/centrifugation procedure was repeated for at least three times. The pH values were measured using a standard pH meter (PHM82, Radiometer Copenhagen) at room temperature. Protein concentrations were determined photometrically by measuring the absorbance at 280 nm (LSAQ: $\epsilon_{280\text{nm}, 1\text{ cm}} = 0.855 \text{ ml/mg}$, LSBS: $\epsilon_{280\text{nm}, 1\text{ cm}} = 0.585 \text{ ml/mg}$).

The synchrotron radiation X-ray scattering data were collected following standard procedures using the $\times 33$ camera of the EMBL on the storage ring DORIS III of the Deutsches Elektronen Synchrotron (DESY).³² The measurements were done in two experimental sessions. For the first session a linear multiwire proportional detector at a sample-detector distance of 2.4 m and a wavelength $\lambda = 0.15 \text{ nm}$, covering a momentum transfer range of $0.13 < s < 3.0 \text{ nm}^{-1}$ was used. The second session was done at the same sample-detector distance and the same wavelength, using a MAR345 two-dimensional image plate detector (the range of momentum transfer was $0.13 < s < 4.2 \text{ nm}^{-1}$). The focusing geometry and narrow wavelength band pass ($\Delta\lambda/\lambda \approx 0.005$) resulted in negligible smearing effects. The pre-thermostated samples were injected into a thermostated silver cell with mica windows with a cell volume of 100 μl and an optical path length of 1 mm. The temperature was controlled within $\pm 0.2^\circ\text{C}$ using a water bath. To check for radiation damage, the data were collected in 15 successive 1 min frames; for the image plate, two 3 min exposures were compared. These measurements indicated no changes in the scattering patterns with time, i.e. there was no measurable radiation damage. The data were averaged after normalization to the intensity of the incident beam and corrected for the detector response. The scattering of the buffer was subtracted using the program package PRIMUS.²⁷ Each sample was measured at two different concentrations ($1.5 \div 2 \text{ mg/ml}$ and $8 \div 10 \text{ mg/ml}$), and no concentration-dependent change was observed. The low and high concentration data were merged for the subsequent data analysis.

The forward scattering $I(0)$ and the radius of gyration R_g were evaluated using the Guinier approximation assuming that at very small angles ($s < 1.3/R_g$) the intensity is represented as $I(s) = I(0) \exp(-(sR_g)^2/3)$. These parameters were also computed from the entire scattering patterns using the indirect transform package GNOM,²⁶ which also provides the distance distribution function $p(r)$ of the particle computed from the transformation:

$$I(s) = 4\pi \int_0^{D_{\max}} p(r) \frac{\sin sr}{sr} dr \quad (1)$$

where D_{\max} is the maximum diameter of the largest particle in the mixture. The maximum diameters were estimated for each scattering data set individually by successive computations with different D_{\max} values. The values for R_g evaluated from the Guinier approximation practically coincided with those computed by GNOM. The molecular masses ($M_{W,\text{exp}}$) of the solutes were evaluated by comparison of the forward scattering with that from reference solutions of bovine serum albumin ($M_W=66$ kDa).

Low-resolution model shape analysis of the SAXS data was done using the *ab initio* program DAMMIN.³³ The program represents the particle as a collection of $M \gg 1$ densely packed beads inside a sphere with the diameter D_{\max} . Each bead belongs either to the particle or to the solvent, and the shape is described by a binary string of length M . Starting from a random string, simulated annealing is employed to search for a compact model that fits the shape scattering curve $I(s)$ to minimize discrepancy:

$$\chi^2 = \frac{1}{N-1} \sum_j \left[\frac{I(s_j) - cI_{\text{calc}}(s_j)}{\sigma(s_j)} \right]^2 \quad (2)$$

where N is the number of experimental points, c is a scaling factor and $I_{\text{calc}}(s)$ and $\sigma(s_j)$ are the calculated intensity and the experimental error at the momentum transfer s_j , respectively. Following the Porod's law³⁴ for homogeneous particles, prior to shape analysis by DAMMIN a constant is subtracted from each data point to force the s^{-4} decay of the intensity at higher angles yielding the resulting "shape scattering" curve. For the analysis of LS particles, DAMMIN was further developed to enable the modelling of icosahedral particles by imposing the icosahedral symmetry into the generation of the beads defining the search volume. The symmetry was incorporated into the model as a rigid constraint, so that all steps during simulated annealing were performed according to the icosahedral symmetry rules.³⁵

For the analysis of mixtures composed by LS aggregates the experimental scattering intensity $I(s)$ from a mixture of K non-interacting components was represented as:

$$I(s) = \sum_{j=1}^K v_j \cdot I_j(s) \quad (3)$$

where v_j and $I_j(s)$ are the volume fraction and the scattering intensity from the j th component, respectively ($0 \leq v_j \leq 1$). The program MIXTURE²⁷ was modified into MIXTURE-M in such a way that it could use not only the simple bodies modeling (e.g., hollow spheres) but also high-resolution models. For the mixtures consisting of high-resolution models of LS assemblies, theoretical scattering curves $I_j(s)$ from the components were calculated using the program CRYSTAL.³⁶ The size of the high-resolution model component could be changed by rescaling the angular axis to the appropriate order and the polydispersity effect could be applied. Based on the results of *ab initio* modeling and the shape of the scattering curves the model containing five components was chosen. It included complete and incomplete icosahedral capsids corresponding to 75 Å and 150 Å radii as well as pentamer components (the use of other models for the small particles did not significantly influence the results).

The theoretical scattering intensities from this model were computed using the program MIXTURE-M,²⁷ which varies the volume fractions of the components in the mixture as well as their radii and polydispersity to minimize discrepancy (2). MIXTURE-M employs a nonlinear fitting procedure based on a gradient method with simple bounds on the parameters. A variation of up to

30 Å in diameters was taken into account for the calculations and the degree of polydispersity for complete capsids was allowed to vary from 0.1 Å to 5 Å, whereas for incomplete structures it was varying from 0.1 Å to 30 Å.

Computer modelling of quasi-equivalent icosahedral capsids

In order to construct the quasi-equivalent capsids, a hexamer model was generated by inserting an extra subunit into the original pentamer from the $T=1$ capsid. The positions of the six subunits were fine adjusted so that the subunit interface was as similar as possible to that of the original pentamer. A certain number of hexamers were then inserted into the proper positions of an enlarged $T=1$ capsid according to the quasi-equivalent geometry. The size and curvatures of the large capsid models were optimized in order to, on one hand avoid severe clashes, on the other hand maintain reasonable subunit contact interface. The final model of the $T=3$ icosahedral capsids consists of 180 subunits with a diameter of 275(±10) Å and the $T=4$ model consists of 240 subunits with a diameter of 320(±10) Å. These models were constructed using the program O.³⁷ The rotation matrices were generated using the program CONVROT (W. Meining)[†].

Acknowledgements

We gratefully acknowledge the continuous support of Dr Michel Koch, EMBL Outstation, Hamburg. This work was supported the Deutsche Forschungsgemeinschaft, the Fonds der Chemischen Industrie and the Hans-Fischer-Gesellschaft. X.Z. and W.M. are grateful for financial support from the European Community - Research Infrastructure Action under the FP6 "Structuring the European Research Area Programme" contract number RII3/CT/2004/5060008, to access the ×33 EMBL beamline at DESY.

References

- Huber, R. (1979). Conformational flexibility and its functional significance in some protein molecule. *Trends Biochem. Sci.* **4**, 271–274.
- Huber, R. & Bennett, W. S., Jr (1983). Functional significance of flexibility in proteins. *Biopolymers*, **22**, 261–279.
- Caspar, D. L. D. & Klug, A. (1962). Physical principles in the construction of regular virus. *Cold Spring Harbor Symp. Quant. Biol.* **27**, 1–24.
- Johnson, J. E. & Speir, J. A. (1997). Quasi-equivalent viruses: a paradigm for protein assemblies. *J. Mol. Biol.* **269**, 665–675.
- Bacher, A. & Ladenstein, R. (1990). The lumazine synthase/riboflavin synthase complex of *Bacillus subtilis*. In *Chemistry and Biochemistry of Flavoenzymes* (Müller, F., ed.), vol. 1, pp. 293–316. Chemical Rubber & Co., Boca Raton, Florida.
- Ladenstein, R., Meining, W., Zhang, X., Fischer, M. & Bacher, A. (2004). Metamorphosis of an enzyme. In

[†] <http://chips.csb.ki.se/xray/convrot.html>

- Conformational Proteomics of Macromolecular Architecture: Approaching the Structure of Large Molecular Assemblies and Their Mechanisms of Action* (Cheng, H. & Hammar, L., eds), pp. 198–221, World Scientific Pub. Co., Stockholm.
7. Bacher, A. & Mailander, B. (1978). Biosynthesis of riboflavin in *Bacillus subtilis*: function and genetic control of the riboflavin synthase complex. *J. Bacteriol.* **134**, 476–482.
 8. Ladenstein, R., Schneider, M., Huber, R., Bartunik, H. D., Wilson, K., Schott, K. & Bacher, A. (1988). Heavy riboflavin synthase from *Bacillus subtilis*. Crystal structure analysis of the icosahedral b60 capsid at 3.3 Å resolution. *J. Mol. Biol.* **203**, 1045–1070.
 9. Ladenstein, R., Ritsert, K., Huber, R., Richter, G. & Bacher, A. (1994). The lumazine synthase/riboflavin synthase complex of *Bacillus subtilis*. X-ray structure analysis of hollow reconstituted b-subunit capsids. *Eur. J. Biochem.* **223**, 1007–1017.
 10. Mörtl, S., Fischer, M., Richter, G., Tack, J., Weinkauf, S. & Bacher, A. (1996). Biosynthesis of riboflavin. Lumazine synthase of *Escherichia coli*. *J. Biol. Chem.* **271**, 33201–33207.
 11. Persson, K., Schneider, G., Jordan, D. B., Viitanen, P. V. & Sandalova, T. (1999). Crystal structure analysis of a pentameric fungal and an icosahedral plant lumazine synthase reveals the structural basis for differences in assembly. *Protein Sci.* **8**, 2355–2365.
 12. Meining, W., Mörtl, S., Fischer, M., Cushman, M., Bacher, A. & Ladenstein, R. (2000). The atomic structure of pentameric lumazine synthase from *Saccharomyces cerevisiae* at 1.85 Å resolution reveals the binding mode of a phosphonate intermediate analogue. *J. Mol. Biol.* **299**, 181–197.
 13. Zhang, X., Meining, W., Fischer, M., Bacher, A. & Ladenstein, R. (2001). X-ray structure analysis and crystallographic refinement of lumazine synthase from the hyperthermophile *Aquifex aeolicus* at 1.6 Å resolution: determinants of thermostability revealed from structural comparisons. *J. Mol. Biol.* **306**, 1099–1114.
 14. Gerhardt, S., Haase, I., Steinbacher, S., Kaiser, J. T., Cushman, M., Bacher, A. et al. (2002). The structural basis of riboflavin binding to *Schizosaccharomyces pombe* 6,7-dimethyl-8-ribityllumazine synthase. *J. Mol. Biol.* **318**, 1317–1329.
 15. Morgunova, E., Meining, W., Illarionov, B., Haase, I., Jin, G., Bacher, A. et al. (2005). Crystal structure of lumazine synthase from *Mycobacterium tuberculosis* as a target for rational drug design: binding mode of a new class of purinetrione inhibitors. *Biochemistry*, **44**, 2746–2758.
 16. Braden, B. C., Velikovsky, C. A., Cauerhoff, A. A., Polikarpov, I. & Goldbaum, F. A. (2000). Divergence in macromolecular assembly: X-ray crystallographic structure analysis of lumazine synthase from *Brucella abortus*. *J. Mol. Biol.* **297**, 1031–1036.
 17. Zylberman, V., Craig, P. O., Klinke, S., Braden, B. C., Cauerhoff, A. & Goldbaum, F. A. (2004). High order quaternary arrangement confers increased structural stability to *Brucella* sp. lumazine synthase. *J. Biol. Chem.* **279**, 8093–8101.
 18. Bacher, A., Bauer, R., Eggers, U., Harders, H. & Schneppele, H. (1976). In *Flavins and Flavoproteins* (Singer, T. P., ed.), Elsevier, Amsterdam.
 19. Bacher, A., Ludwig, H. C., Schneppele, H. & Ben-Shaul, Y. (1986). Heavy riboflavin synthase from *Bacillus subtilis*. Quaternary structure and reaggregation. *J. Mol. Biol.* **187**, 75–86.
 20. Fischer, M., Haase, I., Kis, K., Meining, W., Ladenstein, R., Cushman, M. et al. (2003). Enzyme catalysis via control of activation entropy: site-directed mutagenesis of 6,7-dimethyl-8-ribityllumazine synthase. *J. Mol. Biol.* **326**, 783–793.
 21. Zhang, X., Meining, W., Cushman, M., Haase, I., Fischer, M., Bacher, A. & Ladenstein, R. (2003). A structure-based model of the reaction catalyzed by lumazine synthase from *Aquifex aeolicus*. *J. Mol. Biol.* **328**, 167–182.
 22. Karshikoff, A. & Ladenstein, R. (1989). Electrostatic effects in a large enzyme complex: subunit interactions and electrostatic potential field of the icosahedral b60 capsid of heavy riboflavin synthase. *Proteins: Struct. Funct. Genet.* **5**, 248–257.
 23. Fornasari, M. S., Laplagne, D. A., Frankel, N., Cauerhoff, A. A., Goldbaum, F. A. & Echave, J. (2003). Sequence determinants of quaternary structure in lumazine synthase. *Mol. Biol. Evol.* **21**, 97–107.
 24. Ladenstein, R., Bacher, A. & Huber, R. (1987). Some observations of a correlation between the symmetry of large heavy-atom complexes and their binding sites on proteins. *J. Mol. Biol.* **195**, 751–753.
 25. Koch, M. H. J., Vachette, P. & Svergun, D. I. (2003). Small angle scattering: a view on the properties, structures and structural changes of biological macromolecules in solution. *Quart. Rev. Biophys.* **36**, 147–227.
 26. Svergun, D. I. (1992). Determination of the regularization parameter in indirect-transform methods using perceptual criteria. *J. Appl. Crystallogr.* **25**, 495–503.
 27. Konarev, P. V., Volkov, V. V., Sokolova, A. V., Koch, M. H. J. & Svergun, D. (2003). PRIMUS: a Windows PC-based system for small-angle scattering data analysis. *J. Appl. Crystallogr.* **36**, 1277–1282.
 28. Rossmann, M. G. & Erickson, J. W. (1985). Structure and assembly of icosahedral shells. In *Virus Structure and Assembly* (Casjens, S., ed.), pp. 29–74, Jones and Bartlett Publishers, Inc., Boston.
 29. Kis, K., Volk, R. & Bacher, A. (1995). Biosynthesis of riboflavin. Studies on the reaction mechanism of 6,7-dimethyl-8-ribityllumazine synthase. *Biochemistry*, **34**, 2883–2892.
 30. Bacher, A. (1986). Heavy riboflavin synthase from *Bacillus subtilis*. *Methods Enzymol.* **122**, 192–199.
 31. Xing, L., Kato, K., Li, T., Takeda, N., Miyamura, T., Hammar, L. & Cheng, R. H. (1999). Recombinant hepatitis E capsid protein self-assembles into dual-domain T=1 particle presenting native virus epitopes. *Virology*, **5**, 35–45.
 32. Boulin, C. J., Kempf, R., Gabriel, A. & Koch, M. H. J. (1988). Data acquisition systems for linear and area X-ray detectors using delay line readout. *Nucl. Instrum. Meth. A*, **269**, 312–320.
 33. Svergun, D. I. (1999). Restoring low resolution structure of biological macromolecules from solution scattering using simulated annealing. *Biophys. J.* **76**, 2879–2886.
 34. Porod, G. (1982). General theory. In *Small Angle Scattering* (Glatter, O. & Kratky, O., eds), pp. 17–51, Academic Press, London.
 35. Konarev, P. V., Petoukhov, M. V., Volkov, V. V. & Svergun, D. I. (2006). ATSAS 2.1, a program package for small-angle scattering data analysis. *J. Appl. Crystallogr.* **39**, 277–286.
 36. Svergun, D. I., Barberato, C. & Koch, M. H. J. (1995). CRYSTOL - a program to evaluate X-ray solution scattering of biological macromolecules from atomic coordinates. *J. Appl. Crystallogr.* **28**, 768–773.
 37. Jones, A. T., Zou, J. Y., Cowtan, K. Y. & Kjeldgaard, M. (1991). Improved methods for building protein

- models in electron density maps and the location of errors in the model. *Acta Crystallog. sect. A* **47**, 110–119.
38. Ritsert, K., Huber, R., Turk, D., Ladenstein, R., Schmidt-Bäse, K. & Bacher, A. (1995). Studies on the lumazine synthase/riboflavin synthase complex of *Bacillus subtilis*: crystal structure analysis of reconstituted, icosahedral b-subunit capsids with bound substrate analogue inhibitor at 2.4 Å resolution. *J. Mol. Biol.* **253**, 151–167.
39. Sayle, R. A. & Milner-White, E. J. (1995). RASMOL: biomolecular graphics for all. *Trends Biochem. Sci.* **20**, 374.

Edited by R. Huber

(Received 12 May 2006; received in revised form 14 July 2006; accepted 19 July 2006)
Available online 28 July 2006